X-ray spectrum optimization of full-field digital mammography: Simulation and phantom study

Philipp Bernhardt,[a] Thomas Mertelmeier, and Martin Hoheisel
Siemens AG, 91050 Erlangen, Germany

(Received 20 January 2006; revised 20 July 2006; accepted for publication 9 August 2006; published 26 October 2006)

In contrast to conventional analog screen-film mammography new flat detectors have a high dynamic range and a linear characteristic curve. Hence, the radiographic technique can be optimized independently of the receptor exposure. It can be exclusively focused on the improvement of the image quality and the reduction of the patient dose. In this paper we measure the image quality by a physical quantity, the signal difference-to-noise ratio (SDNR), and the patient risk by the average glandular dose (AGD). Using these quantities, we compare the following different setups through simulations and phantom studies regarding the detection of microcalcifications and tumors for different breast thicknesses and breast compositions: Monochromatic radiation, three different anode/filter combinations: Molybdenum/molybdenum (Mo/Mo), molybdenum/rhodium (Mo/Rh), and tungsten/rhodium (W/Rh), different filter thicknesses, use of anti-scatter grids, and different tube voltages. For a digital mammography system based on an amorphous selenium detector it turned out that, first, the W/Rh combination is the best choice for all detection tasks studied. Second, monochromatic radiation can further reduce the AGD by a factor of up to 2.3, maintaining the image quality in comparison with a real polychromatic spectrum of an x-ray tube. And, third, the use of an anti-scatter grid is only advantageous for breast thicknesses larger than approximately 5 cm. © *2006 American Association of Physicists in Medicine*. [DOI: 10.1118/1.2351951]

Key words: full-field digital mammography, spectrum optimization, signal difference-to-noise ratio, average glandular dose

I. INTRODUCTION

Several commercial full-field digital mammography systems are available today. The main difference to their analog screen-film counterparts is the digital image receptor. In most cases, at least in the case of the nonscanning systems, the x-ray tube is the same as in the corresponding screen-film systems. However, digital detectors usually have different absorption characteristics than the converter screen in an analog system. In digital systems, image acquisition can be optimized separately from the image display. Thus, a possibly suboptimal image contrast could be compensated for by image processing algorithms. This offers the opportunity of designing a system where the issues of image quality and applied dose can be treated independently. Therefore, it may be questioned whether the anode/filter combination molybdenum/molybdenum (Mo/Mo), which is considered the optimal choice for screen-film mammography, is also best suited for digital mammography.

For analog screen-film mammography systems the question of the x-ray spectrum was addressed by Thilander-Klang *et al.*[1] in a clinical study. Compared to the anode-filter combination of molybdenum/molybdenum (Mo/Mo), a molybdenum/rhodium (Mo/Rh), and a tungsten/rhodium (W/Rh) spectrum helped to reduce the absorbed dose considerably—up to 50%—for large compressed breast thickness. These findings were confirmed by the Monte-Carlo studies of Dance *et al.*[2] investigating analog and CR systems with image receptors based on gadolinium oxysulfide screens. That publication also included rhodium/rhodium (Rh/Rh) spectra, which led to findings similar to those when using the W/Rh beam quality.

For digital mammography with flat detectors, Berns, Hendrick, and Cutter[3] conducted a contrast-detail study using an indirect detection technology with CsI as a converter, reporting on the optimization of technique factors and providing a comparison with screen-film mammography. It was found that the larger the breast thickness the greater the advantages of spectra other than that of Mo/Mo. Also Huda *et al.*[4] investigated dose and image quality for a CsI-based digital detector, but considered Mo/Mo beam quality only.

A complete mammography imaging system was modeled by Fahrig and Yaffe.[5,6] With their simulation tool they demonstrated that, in the case of a digital detector based on a Gd_2O_2S scintillator, a tungsten target has advantages for the detection of infiltrating ductal carcinoma and calcifications over a molybdenum target. Using this model, Fahrig *et al.*[7] addressed the optimization of x-ray spectra for a digital mammography detector based on selenium for the first time. An important result was that the optimal spectral conditions for selenium are similar to those of Gd_2O_2S including the possible use of a Mo spectrum.

Flynn *et al.*[8] investigated the issue of an optimized radiographic technique for a detector based on amorphous selenium taking into account Mo and W anodes and several filter materials. Using a simulation technique, they found a tungsten anode with a tin filter optimal for imaging small calcifications.

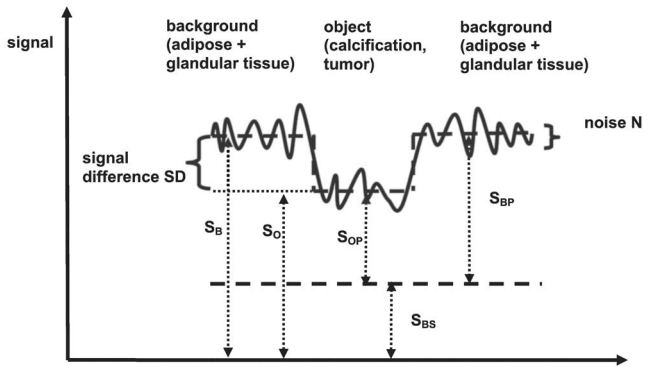

FIG. 1. Definition of the image quality measure: signal difference-to-noise ratio (SDNR) and graphical explanation for the used variables to calculate SDNR.

TABLE I. Number of quanta per tube charge [mAs] and solid angle [sr] as a function of the tube voltage for molybdenum and tungsten anode material (anode angle 20°, filter material 1 mm Be).

Tube voltage	Molybdenum anode Quanta/(mAs sr)	Tungsten anode Quanta/(mAs sr)
18 kV	1.90×10^{11}	4.92×10^{11}
22 kV	3.31×10^{11}	7.39×10^{11}
26 kV	5.46×10^{11}	1.11×10^{12}
30 kV	8.18×10^{11}	1.50×10^{12}
34 kV	1.12×10^{12}	1.91×10^{12}
38 kV	1.46×10^{12}	2.33×10^{12}
42 kV	1.90×10^{12}	2.84×10^{12}

In this paper, we report on simulations taking into account the complete imaging chain of an amorphous selenium full-field digital mammography (FFDM) system. We focus on those anode/filter combinations that are available in the Siemens Novation^{DR} FFDM system, i.e., Mo/Mo, Mo/Rh, and W/Rh, and that have been used in a small phantom study for comparison. A comprehensive phantom study carried out with this system will be published elsewhere.[9,10] For reference and comparison we also give the results obtained for monochromatic radiation.

II. METHODS

A. Image quality measure

To measure the detectability of an object such as a calcification or a tumor in an x-ray image, the signal difference-to-noise ratio (SDNR) is used.[8,11] It is here defined as the ratio between the mean signal difference of the object of interest S_O and the background S_B, and the standard deviation of the noise σ_B in the background (Fig. 1)

$$\mathrm{SDNR} = \frac{S_B - S_O}{\sigma_B}. \tag{1}$$

The noise is averaged over an area, which has the same size as the object of interest. This definition has the advantage of being independent of linear image processing routines, such as the changing of the contrast window and level settings.

In this work the x-ray spectrum is optimized and the benefit of an anti-scatter grid is analyzed. Since both have a rather limited influence on the resolution of the x-ray image, there is no need to analyze the signal difference-to-noise ratio in the frequency space.[12,13]

Since image quality can be improved by applying a higher dose as long as the image noise is dominated by quantum noise, image quality has to be set in relation to the patient dose, i.e., in mammography, to the average glandular dose (AGD). As a measure for the AGD, in the simulations we use the total absorbed dose in the phantom. Therefore, we define a figure of merit Q

$$Q := \frac{(\mathrm{SDNR})^2}{\mathrm{AGD}}. \tag{2}$$

This is the quality factor we use to find the optimal radiographic technique for the system under investigation.

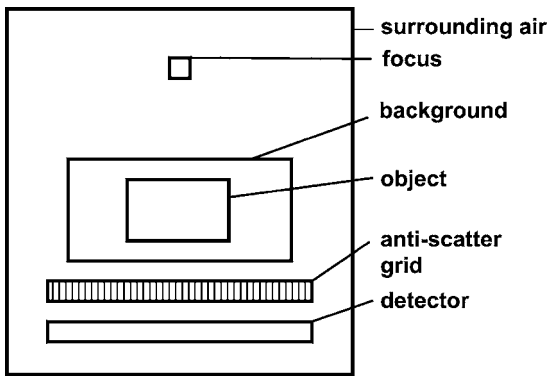

FIG. 2. Geometrical setup of the simulations.

B. Simulations

1. Geometrical model

The geometrical model for the simulations is given in Fig. 2. The almost point-like focal spot emits radiation isotropic into the direction of the detector. The background material, representing the breast, is modeled as a cube with a defined thickness. The object itself is represented by a cylinder with a certain radius, which is placed directly at the center of the cube. An optionally employed linear anti-scatter grid is simulated by alternating strips of high and low absorbing material, which are aligned to the focal spot. The motion of the grid vertically to the x-ray beam is considered by randomly positioning every simulated quantum in the range of the size of a one-dimensional (1D) unit cell (sum of the width of one low and one high absorbing strip). The detector itself is described by the highly absorbing cube with an active surface of defined density. The entire arrangement is put into an air ambient.

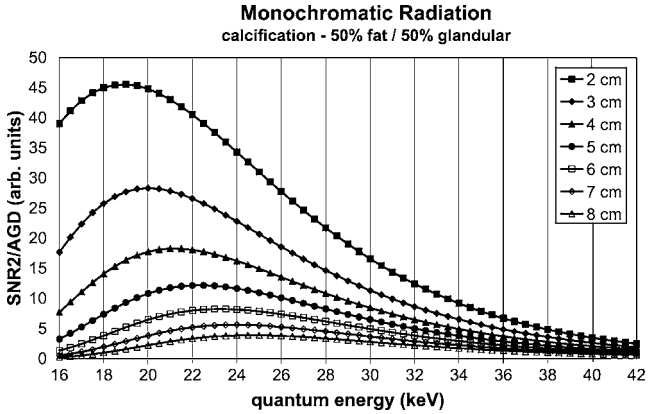

FIG. 3. Quality factor Q for monochromatic radiation for the detection of calcifications for different breast thicknesses. The breast phantom consists of 50% adipose and 50% glandular tissue.

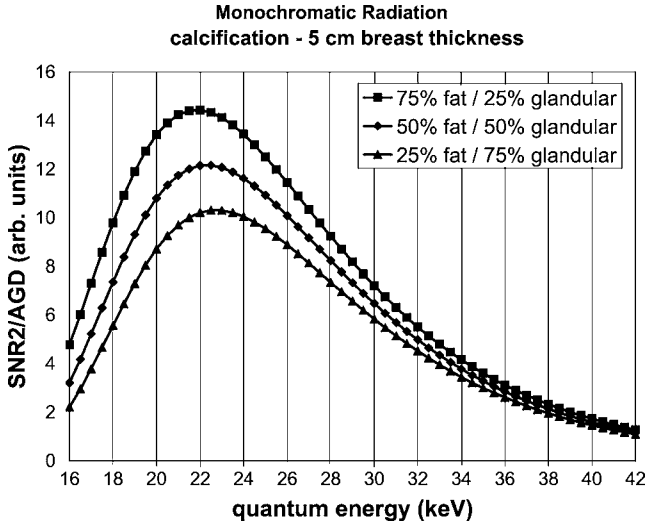

FIG. 5. Quality factor Q for monochromatic radiation for the detection of calcifications for a breast thickness of 5 cm with different adipose/glandular composition.

2. Input parameters

The input parameters for the simulations are closely related to the Siemens full-field digital mammography system Novation^{DR}, based on a direct converting amorphous selenium detector.

General geometry:

- source-to-image distance (SID): 650 mm;
- air gap between background cube and detector: 15 mm.

Source:

- molybdenum anode, tungsten anode;
- quantum flux: See Table I;
- maximum power: 3.75 kW (molybdenum), 4.70 kW (tungsten);
- tube voltage: 16–42 kV (for simulation only; the Novation^{DR} system uses 23–35 kV);
- pre-filter: 1 mm Be.

Filter

- molybdenum filter;
- rhodium filter.

Anti-scatter grid:

- Siemens moving mammography anti-scatter grid;
- spacing material: paper;
- absorbing material: lead;
- cover material: carbon fiber.

Phantom background cube:

- thickness: 20, 30, 40, 50, 60, 70, and 80 mm;
- glandular tissue,[14] density: 1.05 g/cm^3;
- adipose tissue,[14] density: 0.98 g/cm^3.

Contrast object material:

- calcification: $Ca_5P_3O_{13}H$,[15] density: 3.2 g/cm^3, thickness: 0.2 mm;

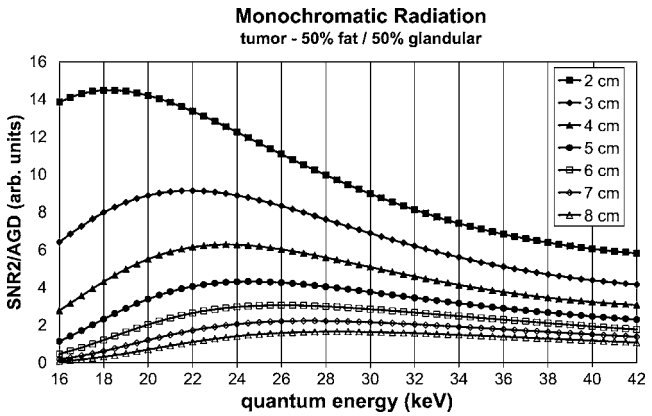

FIG. 4. Quality factor Q for monochromatic radiation for the detection of tumors for different breast thicknesses. The breast phantom consists of 50% adipose and 50% glandular tissue.

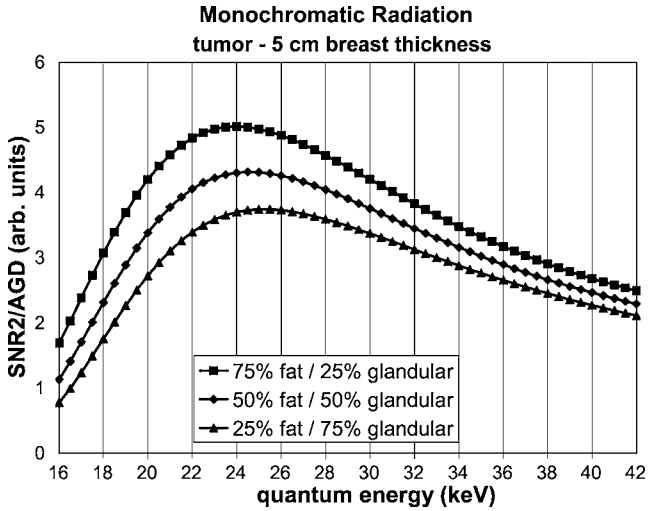

FIG. 6. Quality factor Q for monochromatic radiation for the detection of tumors for a breast thickness of 5 cm with different adipose/glandular composition.

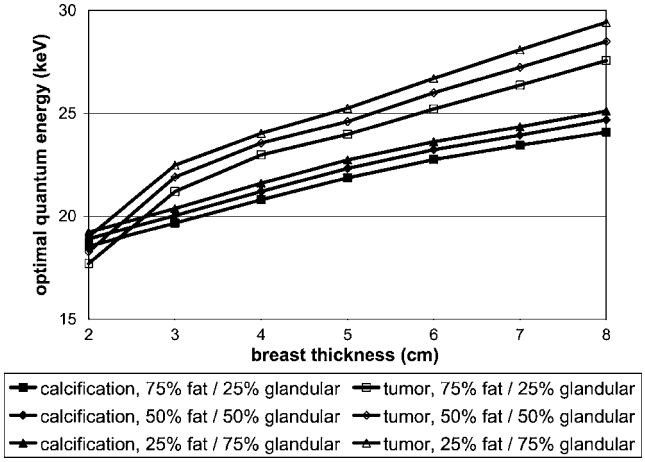

FIG. 7. Optimal quantum energy for the detection of calcifications and tumors in dependence on the breast thickness for monochromatic radiation. The lines just guide the eyes.

- tumor: material composition equivalent to glandular tissue,[16] density: 1.044 g/cm^3, thickness: 5.0 mm.

Detector:

- pixel size: 0.07 mm $\times$ 0.07 mm;
- detector size: 23 cm $\times$ 29 cm corresponding to 3328 $\times$ 4096 pixels;
- absorber: direct converting amorphous selenium, thickness: 0.25 mm, density: 4.28 g/cm^3.

These parameters are typical for mammographic flat detectors based on amorphous selenium. Other detector layers and structures are considered to have little influence on the detection process. It can be assumed that these simulations are of general validity for such systems.

3. Calculation of image quality measure

Simulating real images by ray tracing using a Monte Carlo method would be very demanding, even with the power of today's computers. Therefore, the determination of the SDNR value is divided into two parts: A deterministic and a stochastic simulation. The deterministic simulation calculates, for every detector pixel the signal intensity for the primary radiation for a given spectrum and geometrical setup, neglecting the effects of different interaction processes of the quanta and the subsequent scattered radiation. This calculation can be done for both monochromatic and polychromatic spectra. The spectra are taken from Boone *et al.*[17,18] With the help of the generated images the primary signal intensity of the object S_{OP} and the background S_{BP} can be determined (Fig. 1).

The stochastic simulation, in contrast, is based on Monte Carlo techniques. Here, the complete history of randomly chosen x-ray quanta is tracked, including all photon scatter processes (photon absorption, coherent scattering, Compton scattering, K-fluorescence). For the stochastic simulations the contrast object is omitted, since only the properties of the background are investigated. In the following, the subscripts B,O,P,S refer to the "background region", the "object region", the "primary quanta", and the "secondary quanta", respectively. If P or S is omitted, the "sum of primary and secondary quanta" is addressed. If a sufficiently large number of quanta is simulated, the average glandular dose AGD, the number of detected primary and secondary quanta per pixel N_{BP} and N_{BS}, and the signal intensity S_{BS} of the scatter radiation in the background (Fig. 1) can be extrapolated with the help of the correspondent quantum flux (see Table I) of the source. The resulting scatter to primary ratios have been published elsewhere.[19] Both simulations are done with Siemens' internal software package "DRASIM" and "MOCASSIM," written by Stierstorfer *et al.*[20]

The noise variance σ_B^2 in the background can then be calculated by

$$\sigma_B^2 = \frac{S_{BP} + S_{BS}}{\sqrt{N_{BP} + N_{BS}}}, \tag{3}$$

assuming that Poisson statistics can be applied and neglecting the effect of the additional noise of the energy distribution of the quanta.

Since the scatter radiation, in the case of a sufficiently small object, is distributed virtually homogeneously across the whole image, the SDNR is given by

$$\mathrm{SDNR} = \frac{S_B - S_O}{\sigma_B} = \frac{(S_{BP} + S_{BS}) - (S_{OP} + S_{BS})}{\sigma_B} = \frac{S_{BP} - S_{OP}}{\sigma_B}. \tag{4}$$

The calculation of the SDNR value can now be carried out for a large parameter space, e.g., different tube voltages, anode materials, or filter thicknesses to determine the optimal configuration for a given detection task.

To estimate the stochastic errors of the results of the simulations, the stochastic calculations were repeated five times, starting with different seed values for the random number generator. In all cases, standard deviation of the results was not larger than 2%, hence error bars in the plots are omitted.

C. Phantom measurements

Accompanying the simulations, we carried out phantom measurements. The objective was twofold. One goal is to find the optimal exposure settings, i.e., radiographic technique, as a function of tube voltage in the range between 23 and 35 kV using the full-field digital mammography unit Siemens Mammomat Novation^{DR}. It is not *a priori* clear that the exposure tables applied in an analog screen-film system represent the appropriate technique for a digital system. Another purpose of the phantom measurements was the verification of the simulation results for the parameter subspace that is accessible by the system.

The signal difference-to-noise ratio and an estimate for the average glandular dose were used to determine the quality factor as outlined in Sec. II A.

Breast equivalent phantoms with 50% adipose, 50% glandular tissue of various thicknesses from 2 to 8 cm with a 0.1 mm thick aluminum sheet on top were used to determine

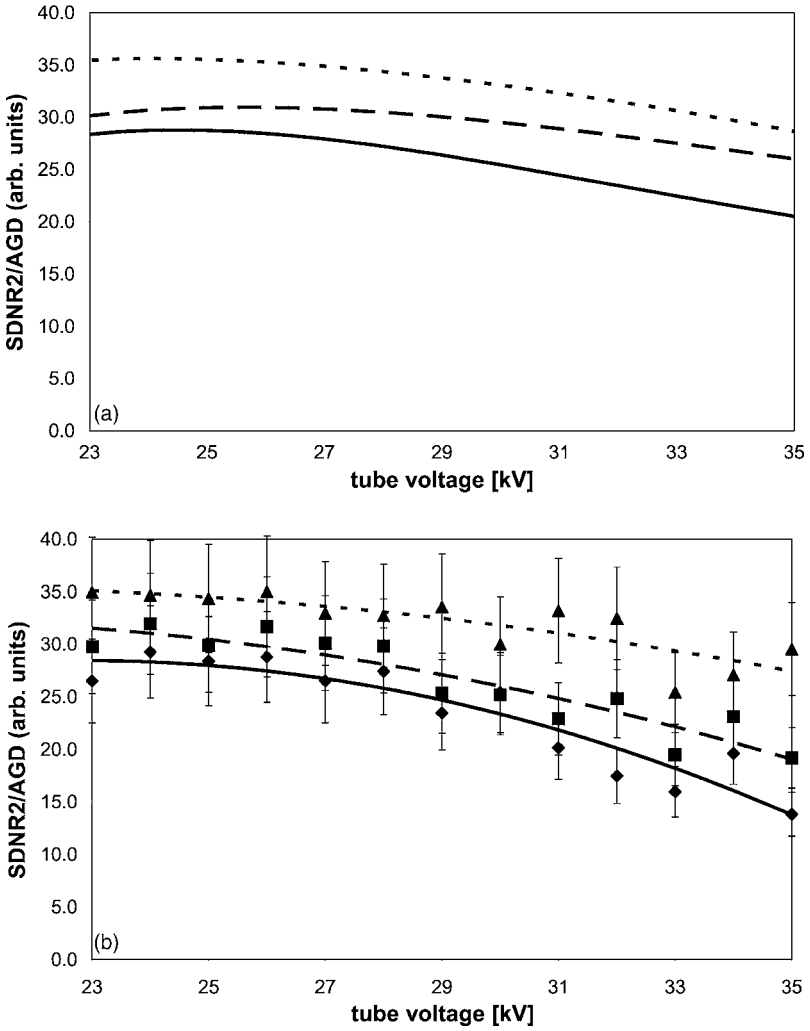

FIG. 8. Quality factor Q for real spectra for the detection of calcifications in dependence on the tube voltage for a breast thickness of 2 cm. The breast phantom consists of 50% adipose and 50% glandular tissue. Solid line/diamonds: Mo/30 μm Mo, dashed line/squares: Mo/25 μm Rh, dotted/triangles: W/50 μm Rh. (a) simulation, (b) phantom experiment. Polynomial curves of second order through the measurement data have been fitted to guide the eye. The uncertainty in the measurement results is estimated to be 15%, the uncertainty for the simulations is smaller than 2%.

the SDNR. The aluminum sheet was assumed to mimic a microcalcification since their attenuation coefficients are rather similar.[21] The diameter of the sheet was large in comparison to typical microcalcifications. This is necessary to be able to determine the signal and noise with sufficient precision. On the other hand, resolution is not considered in this work. Hence, the results do not depend on the size of the observed objects.

For all exposures, the entrance surface air kerma was measured with a Solidose model 400 dosimeter (RTI Electronics AB, Sweden) in the entrance plane of the phantom. The mean glandular dose (AGD) was calculated from the measured exposure according to Dance *et al.* (1990).[22]

The SDNR was calculated using the raw images (processed only with the usual gain, offset, and defective pixel correction, but not postprocessed) according to Eq. (1) with S_O denoting the digital signal (pixel value) underneath the aluminum sheet as the object and S_B being the digital signal value of the background (breast equivalent tissue). The standard deviation was calculated from the background signal in a region-of-interest of the same size (128×128) used for calculating the signals S_O and S_B. From the SDNR and the AGD the figure of merit according to Eq. (2) was calculated.

To give an estimate of the measurement uncertainty, we carried out an error propagation calculation using the following assumptions. According to the quality control manual for the device (Siemens Novation^{DR}, Siemens Medical Solutions, Erlangen) the uncertainty (coefficient of variation) of the pixel values shall be smaller than 5%. The uncertainty of the dose measurement is specified to be 5% (RTI Electronics AB, Sweden). Thus the error propagation for the figure of merit [Eq. (2)] leads to an estimated uncertainty of 15%.

III. RESULTS

A. Simulation

1. Monochromatic spectra

To understand the characteristics required of a spectrum suitable for a given detection problem (object, breast thickness, breast composition) the first simulation runs were conducted with a monochromatic spectrum in the range between 16 and 42 keV. Here filtering could be neglected as well as restriction of the source. The anti-scatter grid was included. The usability of a certain quantum energy was measured by the quality factor Q [Eq. (2)]. It was not necessary to make

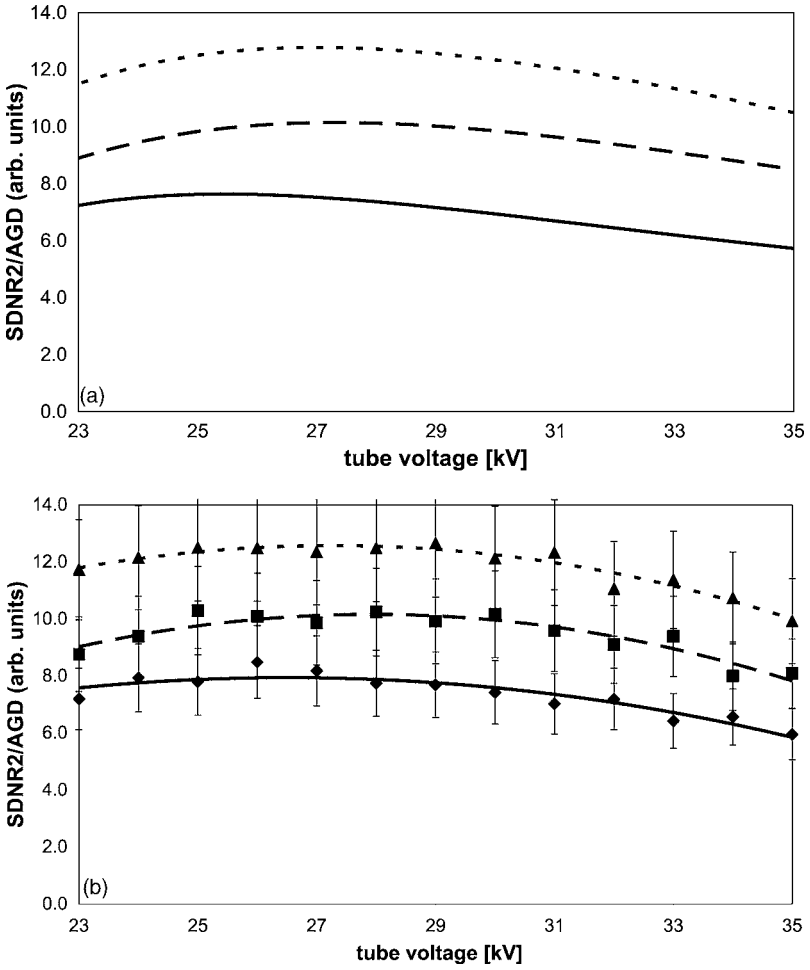

FIG. 9. Quality factor Q for real spectra for the detection of calcifications in dependence on the tube voltage for a breast thickness of 4 cm. The breast phantom consists of 50% adipose and 50% glandular tissue. Solid line/diamonds: Mo/30 μm Mo, dashed line/squares: Mo/25 μm Rh, dotted/triangles: W/50 μm Rh. (a) simulation, (b) phantom experiment. Polynomial curves of second order through the measurement data have been fitted to guide the eye. The uncertainty in the measurement results is estimated to be 15%, the uncertainty for the simulations is smaller than 2%.

an assumption about the quantum flux for a monochromatic source, since both the $(\mathrm{SNDR})^2$ and the AGD are linearly dependent on the quantum flux, hence the value is canceled.

Figures 3 and 4 show the quality factor for the detection of calcifications and tumors, respectively, as function of different quantum energies and breast thicknesses. Here, the breast phantom is assumed to consist of 50% adipose and 50% glandular tissue. It is important to note, that Q is always given in arbitrary units, the simulations do not claim to make any predictions about absolute visibility, since system blurring, resolution, and influences of the human visual system are not considered. In general, the Q values become smaller when the breast thickness increases. In the case of a calcification, the optimum is located at 18.9 keV at a breast thickness of 2 cm. It rises to 24.7 keV for a 8 cm thick breast. In contrast, the optimum energy for tumor tissue rises from 18.3 keV for a 2 cm thick breast to 28.5 keV for a 8 cm thick breast.

In Figs. 5 and 6 the influence of different composition of breast material is investigated for a 5 cm thick breast for the detection of calcifications and tumors. It can be seen, that the adipose-rich breast increases the quality factor Q, i.e., the objects are easier to detect at the same dose load for the patient. On the other hand, the optimal quantum energy is slightly lowered. In Fig. 7 the optimum energies for the detection of calcifications and tumors as function of the breast thickness are summarized.

2. Realistic polychromatic spectra

Realistic polychromatic spectra of three frequently used anode/filter combinations were investigated in the simulations:

- Anode: Molybdenum, filter: Molybdenum, thickness 30 μm;
- Anode: Molybdenum, filter: Rhodium, thickness 25 μm;
- Anode: Tungsten, filter: Rhodium, thickness 50 μm

In Figs. 8(a), 9(a), 10(a), and 11(a) we show the simulation results for the figure of merit Q for microcalcifications in a 50% fatty/50% glandular background as a function of tube voltage for breast thicknesses of 2, 4, 6, and 8 cm for each of these spectra with fixed filter thickness available today in the FFDM system under investigation. It can be seen that, in qualitative agreement with the results of the monochromatic simulations, there is an optimum voltage where the quality factor Q reaches its maximum. But the curves are

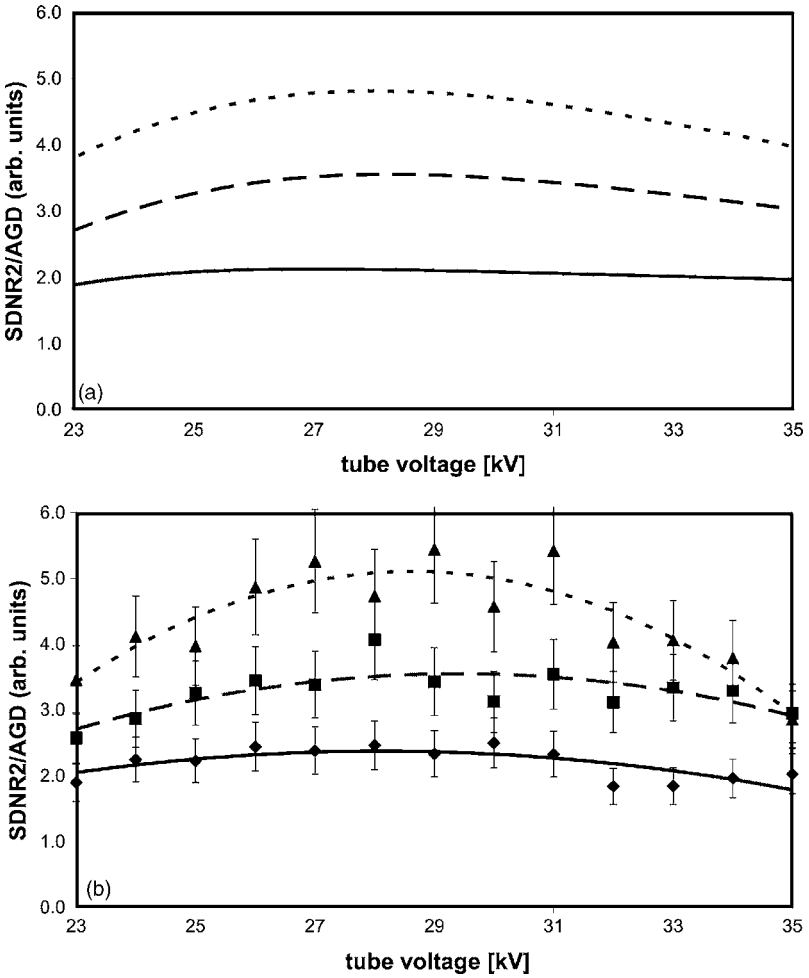

FIG. 10. Quality factor Q for real spectra for the detection of calcifications in dependence on the tube voltage for a breast thickness of 6 cm. The breast phantom consists of 50% adipose and 50% glandular tissue. Solid line/diamonds: Mo/30 μm Mo, dashed line/squares: Mo/25 μm Rh, dotted/triangles: W/50 μm Rh. (a) simulation, (b) phantom experiment. Polynomial curves of second order through the measurement data have been fitted to guide the eye. The uncertainty in the measurement results is estimated to be 15%, the uncertainty for the simulations is smaller than 2%.

rather flat, indicating a relative tolerance against the nonoptimal voltage setting. The most pronounced result, however, is that the curves for W/Rh are always higher than the curves for Mo/Rh, which in turn are higher than those for the Mo/Mo spectrum.

The results for the quality factor of the phantom measurements are plotted in Figs. 8(b), 9(b), 10(b), and 11(b) as function of tube voltage. In a similar manner as the figures for the simulation results [Figs. 8(a), 9(a), 10(a), and 11(a)], the corresponding graphs are shown for each phantom thickness. As the simulations and measurement data cannot be compared quantitatively, the vertical axes of the measurement results have been scaled by an arbitrary factor. The maximum of the figure of merit curves give the optimal kV value settings for each anode/filter combination. A polynomial curve of order 2 has been fitted to each set of measurement data.

If a real x-ray system is designed, optimization of the quality factor Q is not sufficient. A spectrum with a high quality factor tends to have a limited radiation output, particularly if the thickness of the pre-filter is not a fixed parameter. In addition, we choose 1 s as the maximum exposure time for the subsequent simulations. This is driven by the goal to minimize motion blurring. Motion blurring reduces the effective spatial resolution and thus the image quality.[12] Moreover, in first clinical data exposure times below 1 s have proven to be sufficient in most cases.[24]

Hence, the x-ray system is now optimized with respect to the following combined criteria:

- Thin breast: Here it is easy to achieve a very good image quality. Therefore, the SDNR value is fixed to a value which is sufficient for diagnosis, and the average glandular dose should be as low as possible. This case is the "iso-quality" scenario.
- Thick breast: Here the average glandular dose should not exceed a certain value. Hence, optimization tries to get the best image quality for the given maximum average glandular dose. This situation is referred to as the "iso-dose" scenario.

In the following simulations, the maximum SDNR value is set to 2.5 and 1.6 for calcifications and tumors, respectively, and the maximum average glandular dose is 1.5 mGy. This value seems to be rather low compared to that used for screen-film systems. However, the generally improved DQE values of the new digital flat panel detectors may be exploited for dose reduction. Furthermore, this low dose level

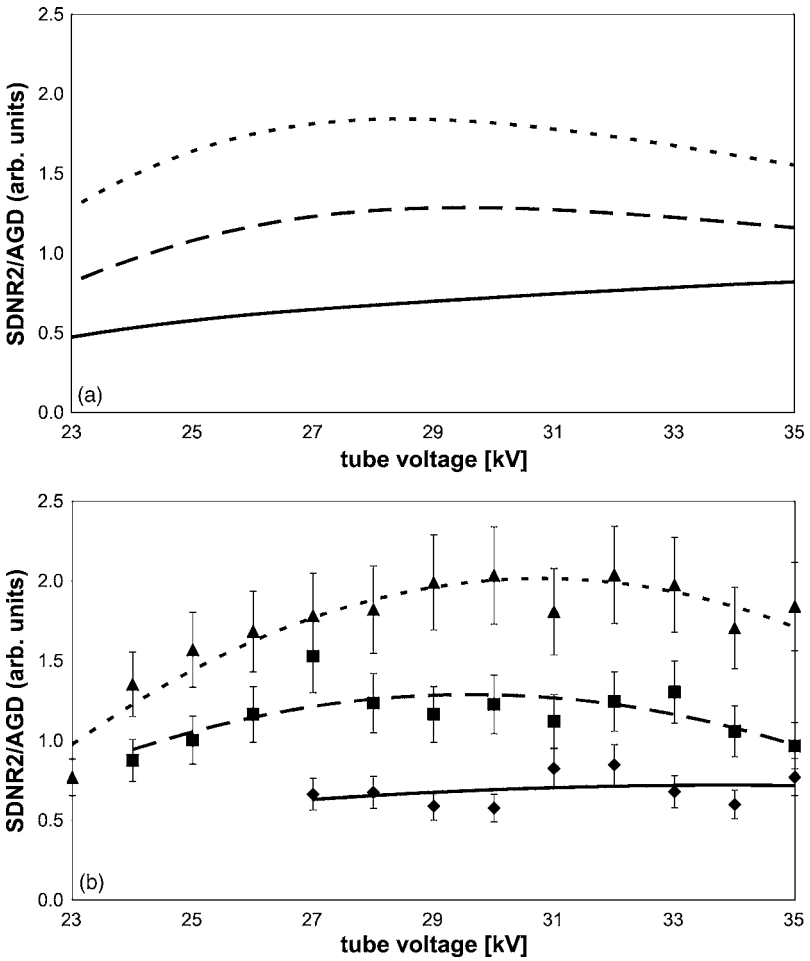

FIG. 11. Quality factor Q for real spectra for the detection of calcifications in dependence on the tube voltage for a breast thickness of 8 cm. The breast phantom consists of 50% adipose and 50% glandular tissue. Solid line/diamonds: Mo/30 μm Mo, dashed line/squares: Mo/25 μm Rh, dotted/triangles: W/50 μm Rh. (a) simulation, (b) phantom experiment. Polynomial curves of second order through the measurement data have been fitted to guide the eye. The uncertainty in the measurement results is estimated to be 15%, the uncertainty for the simulations is smaller than 2%.

seems to be adequate as demonstrated by first clinical data.[24] As already stated above, the SDNR values of the simulations do not permit conclusions to be drawn on the absolute detectabiltity of a certain object. They can only be used to compare different setups. Even a comparison between the visibility of the small calcifications and relatively large tumors on the basis of the Q value defined here is neither possible nor meaningful. The maximum SDNR values are chosen in a way that enables this image quality to be reached for breast thicknesses at approximately 5 cm with the maximum average glandular dose of a low mammography exposure level. The results of the optimization do not claim to be perfectly suited for clinical application.

The exposure parameters have now been optimized for the detection of calcifications and tumors in the parameter space given by breast thickness, with or without grid and fixed or variable filter thicknesses (Figs. 12–17). The fixed filter thicknesses focused on commonly used values, as mentioned above. The breast model consisted of a mixture of 50% adipose and 50% glandular tissue. The results for the optimized exposure parameters, i.e., tube voltage, mAs, and filter thickness, are shown in Table II.

Basically the optimized values follow the results of the monochromatic optimization; the optimum tube voltage rises faster for the detection of tumors than for calcifications. The exposure settings with a variable filter thickness tend to exploit the maximum tube power together with maximum possible filtration. Exposure settings without the anti-scatter grid tend to benefit from lower tube voltages compared to systems with anti-scatter grids. In a number of cases, particularly for Mo/Mo, a large change in the tube voltage between different breast thicknesses can be observed. This is the consequence of the rather short exposure time constraint.

First, we investigated the influence of different anode and filter materials on the detection of calcifications and tumors, respectively (Figs. 12 and 13). An anti-scatter grid was used and the filter thickness was fixed. It was found that the tungsten anode together with the 50 μm rhodium filter delivered the best results for all breast thicknesses and objects. With W/Rh the quality factor could be raised by a factor of up to 1.8 in comparison to the Mo/Mo combination.

Figures 14 and 15 demonstrate the influence of the monochromatization of the spectrum. Here a tungsten anode with a 50 μm rhodium filter and a tungsten anode with variable rhodium filter are compared with an optimized monochromatic spectrum with unlimited power with the quantum energies shown in Fig. 7. A variable filter thickness can increase the Q value up to 16%, whereas a perfect monochromatic spectrum without any pre-filtration can increase Q by a factor of up to of 2.3, particularly for thick breasts.

Finally, Figs. 16 and 17 investigate the influence of an

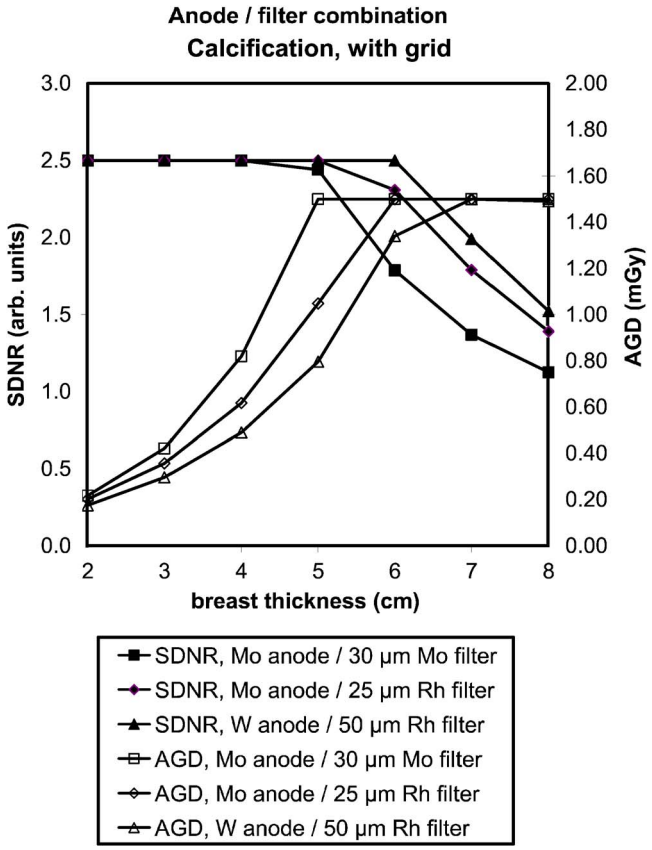

FIG. 12. SDNR values and mean breast doses for the detection of calcifications for different breast thicknesses and anode/filter combinations. The filter thicknesses are fixed. The optimal exposure parameters are given in Table II.

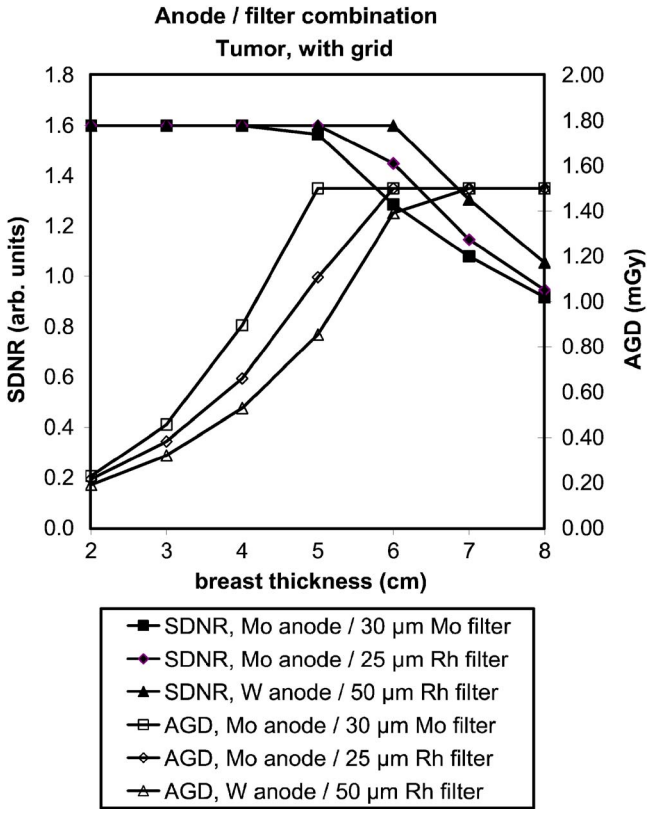

FIG. 13. SDNR values and mean breast doses for the detection of tumors for different breast thicknesses and anode/filter combinations. The filter thicknesses are fixed. The optimal exposure parameters are given in Table II.

anti-scatter grid in digital mammography. Here the results for the SDNR and the mean breast dose are given with and without the grid. It appears that the grid is not advantageous for breast thicknesses up to approximately 4 cm both for the detection of calcification and tumors. Omitting the grid increases the quality factor up to 16% for thin breasts. For thick breasts the use of the anti-scatter grid raises Q up to 26%.

IV. DISCUSSION

A. Monochromatic spectra

For larger breast thicknesses the quantum energy should be raised (Figs. 3 and 4). This is due to the fact that higher energy quanta have a lower absorption cross section, and therefore have a greater chance of reaching the detector. Of great interest is the fact that the detection of tumors requires a higher energy than the detection of calcifications (Fig. 7). This finding is explained in Fig. 18. Here, the mean free path resulting from the simulation is given as a function of quantum energy. It can be seen that the mean free path for calcifications exhibits a greater reduction at lower energy levels compared to the mean free path for tumors. Therefore, the detection of calcifications profits much more from low energy quanta than the detection of tumors.

The better detectability of objects in the case of adipose breasts (Figs. 4 and 6) can be explained by the lower mass density and the increased ratio of carbon to oxygen atoms. Both increase the transmission of the quanta, which facilitates the use of low energy quanta.

B. Realistic polychromatic spectra

The simulations for the monochromatic spectra show that there is one optimum quantum energy for a given detection task. The spectrum of an x-ray tube with given anode and filter material can be influenced by two parameters, the tube voltage and the thickness of the filter. The tube voltage is responsible for the maximum energy of the spectrum, whereas the filter mainly controls the low energy side of the spectrum. Therefore, optimization with real spectra leads to a tube voltage above and close to the optimum quantum energy and to a thick filter, which narrows the spectrum. A limited tube power can be compensated for by increasing the tube voltage and/or decreasing the filter thickness. Both methods broaden the spectrum and result in a reduced quality factor.

The phantom measurement results [Figs. 8(b), 9(b), 10(b), and 11(b)] agree rather well with the simulated figure of merit curves [Figs. 8(a), 9(a), 10(a), and 11(a)] and represent a reasonable confirmation of the theoretical model.

The anti-scatter grid reduces the scatter radiation, but also the primary radiation, thus leading to a reduction in the level

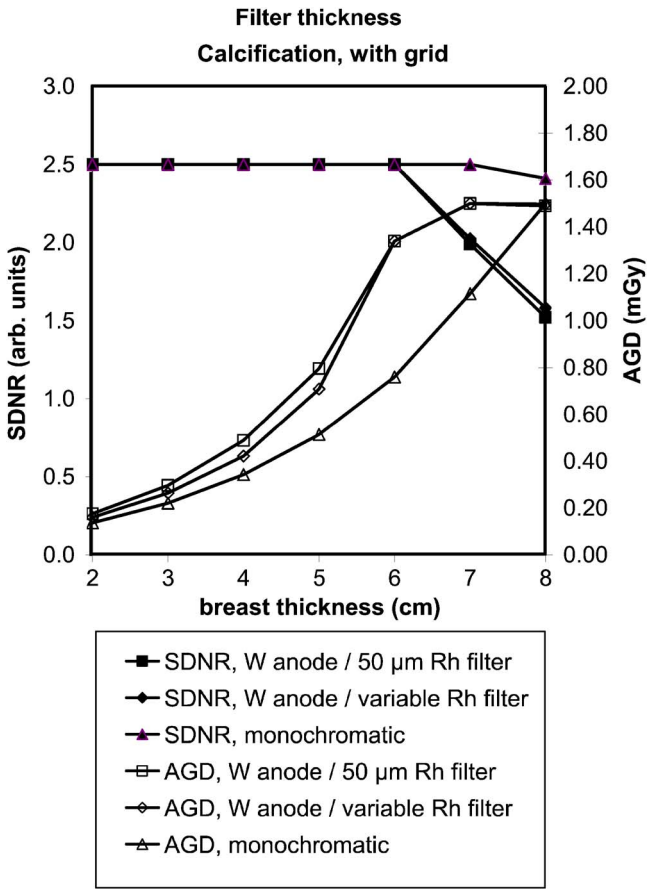

FIG. 14. SDNR values and mean breast doses for the detection of calcifications for different breast thicknesses. A W/Rh system with fixed filter thicknesses, with variable filter thicknesses and a monochromatic spectrum is used. The optimal exposure parameters are given in Table II.

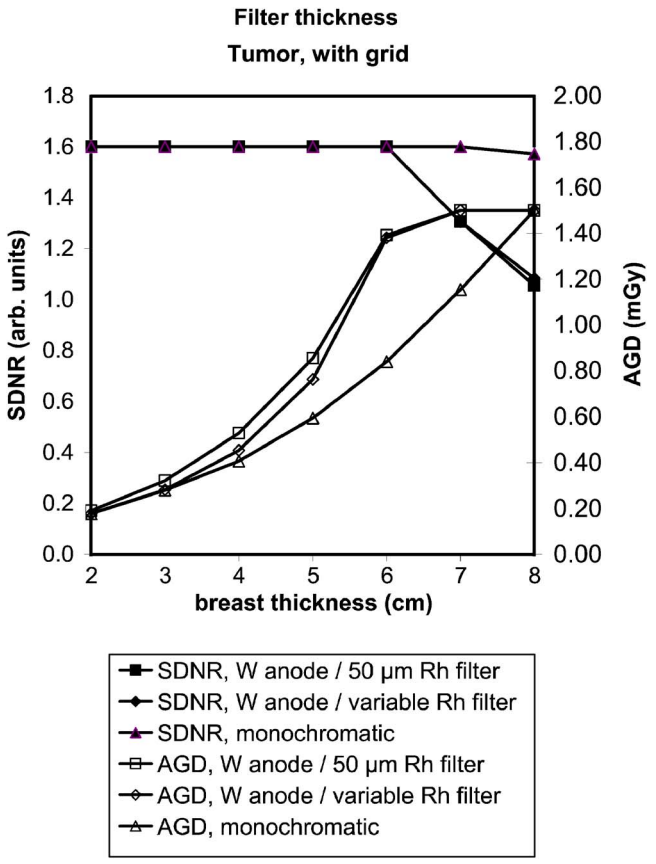

FIG. 15. SDNR values and mean breast doses for the detection of tumors for different breast thicknesses. A W/Rh system with fixed filter thicknesses, with variable filter thicknesses and a monochromatic spectrum is used. The optimal exposure parameters are given in Table II.

of the detected signal. To compensate for this the tube has to deliver a higher photon flux with a slightly increased tube voltage.

The filter materials molybdenum and rhodium with their K absorption edges at 20.0 and 23.2 keV, respectively, are inadequate for the detection of tumors in thick breasts, which requires energies around 28.5 keV. Hence, optimization results in a high tube voltage in order to make the spectrum as hard as possible, however at the price of a considerable broadening of the spectrum.

The advantage of a W/Rh combination for all detection tasks seems to be in contradiction to the experience in conventional analog mammography.[18] If the detector dose is fixed, as in the case of a screen-film system, image quality is improved whenever the quantum energy is lowered, because these quanta deliver a better contrast. Thus, a molybdenum anode with its characteristic peaks at 17.5 and 19.6 keV is most suitable.

However, the digital detectors have a high dynamic range. As in digital mammography, image quality has to be characterized by SDNR and not by relative contrast the detector dose can be varied. This allows contrast loss to be compensated for by reduced noise. Therefore, the spectrum can be designed around quantum energies with an optimum quality factor. This is why the more flexible and powerful tungsten anode delivers better results in digital mammography.[5,6,8,24] The finding that a *W* spectrum, with its higher mean energy, outperforms a Mo spectrum may also be assigned to the fact that higher energy quanta are absorbed more effectively by the selenium layer compared to the thin screen used in film imaging.

Monochromatization by filtering is already extensively used in analog mammography. For example a typical molybdenum filter of 30 μm decreases the number of quanta by 75% for a molybdenum anode with 28 kV. Hence, a further increase of the filter thickness results in small improvements in the monochromatization, however, it increases the scatter radiation, produced by the filter, which is included in this simulation. Furthermore, for thick breasts the tube power is not sufficient for increased filter thickness. Therefore, the advantage of using a variable filter thickness is limited. However, an x-ray source, which produces a monochromatic spectrum on its own, however, would have a considerable impact on the quality factor, particularly for thick breasts.[25]

Finally, we come to the discussion of the influence of the anti-scatter grid. Again, the result obtained seems to be in disagreement with the experience from analog mammography. An image with a fixed detector dose is improved if scatter radiation is replaced by primary radiation. An in-

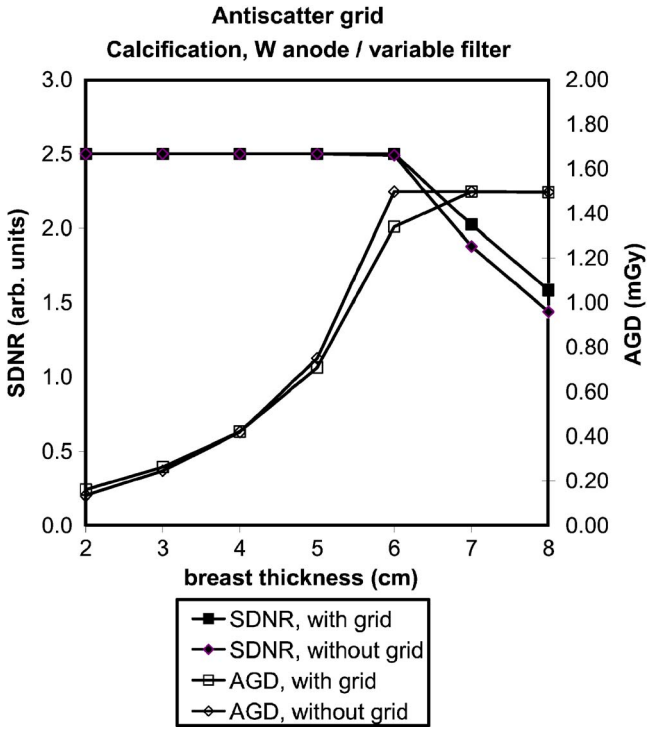

FIG. 16. SDNR values and mean breast doses for the detection of calcifications for different breast thicknesses. A system with and without an anti-scatter grid is used. The optimal exposure parameters are given in Table II.

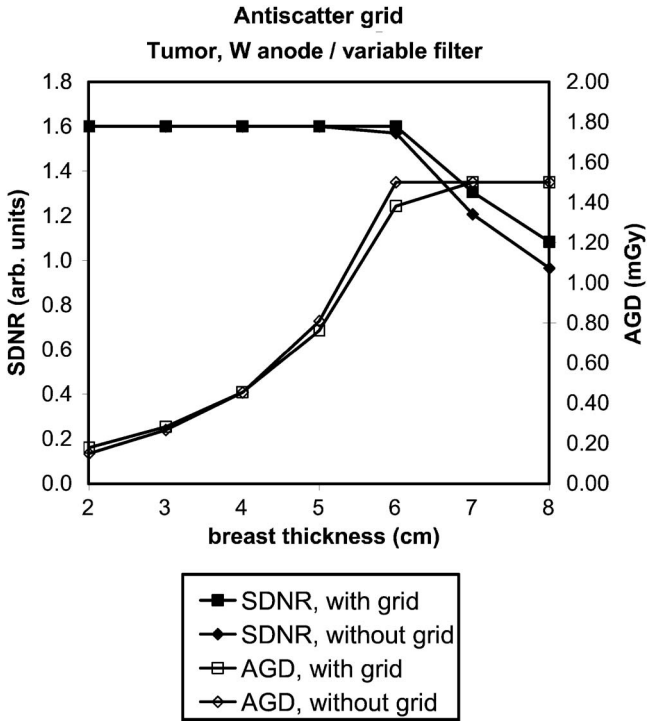

FIG. 17. SDNR values and mean breast doses for the detection of tumors for different breast thicknesses. A system with and without an anti-scatter grid is used. The optimal exposure parameters are given in Table II.

creased dynamic detector range, however, can compensate for an increased amount of scatter radiation by higher detector doses. Radiation with a mammographic spectrum has a very low material penetration. Hence, any kind of additional material in the radiation path, even air, markedly weakens the intensity. Therefore, the grid was modeled in detail, taking into consideration the lamellae and the cover. Under these circumstances it is clear that an anti-scatter grid in digital mammography is only of advantage for breast thicknesses above approximately 5 cm, where the quantity of scatter radiation is high and the spectrum is hard enough to penetrate the anti-scatter grid with ease.[19,26–28]

This paper only deals with simulations and phantom experiments. Our findings have their limitations and cannot be applied quantitatively to clinical images. In clinical images it is not only quantum noise which influences image quality and which is taken into account by our study, but also structural or anatomic noise. This is particularly important for mammography, where tissue overlap may mask structures important for diagnosis. Furthermore, electronic noise is not considered in our study. Physical characterization of the detector has demonstrated[29] that it is quantum noise limited in the range of exposures used for mammography. Above all, a strong electronic noise component would force the system to apply higher detector doses and, hence, higher tube voltages, which would further increase the advantages of a W/Rh system for a digital flat-panel detector.

It can be expected that in clinical images the trend will be very similar to those we have uncovered in these simulation and phantom studies. Nevertheless, future work will have to address the issue of the optimization of radiographic technique for clinical images.

V. CONCLUSION

In this work we optimized the x-ray spectrum for full-field digital mammography to improve the image quality and reduce the patient dose load. We were able to clearly demonstrate that, for every detection task (calcification or tumors, thickness of breast, different breast composition), there is a unique quantum energy which delivers the highest signal difference-to-noise ratio (SDNR) at a given average glandular dose (AGD). Hence, a monochromatic, continuously adjustable x-ray source would be the optimal choice. The best approximation to the ideal monochromatic spectrum can be achieved using a tungsten/rhodium anode/filter combination. The efficiency can be further improved by adjusting the thickness of the pre-filter to the given detection task. For breast thicknesses up to 5 cm, an anti-scatter grid should be omitted as the scatter radiation is low and the penalties in terms of the loss of primary radiation through absorption are high.

Our findings would seem to be at odds with the parameters traditionally employed in analog screen-film mammography setups. However, a film requires a predetermined radiation exposure, which severely limits the optimization in parameter space, whereas a digital detector, in contrast, can work with exposure conditions which cannot be handled by an analog screen-film system.

TABLE II. Optimized exposure parameter (tube voltage (kV), filter thickness (μm) and tube current-time product (mAs) per exposure for different breast thicknesses, for the detection of calcifications and tumors, for fixed and variable filter thicknesses, with and without an anti-scatter grid. The breast phantom consists of 50% adipose and 50% glandular tissue. Optimization criteria are given in the text.

		With anitscatter grid											
		Calcification						Tumors					
		fixed filter			variable filter			fixed filter			variable filter		
		Mo/Mo	Mo/Rh	W/Rh	Mo/Mo	Mo/Rh	W/Rh	Mo/Mo	Mo/Rh	W/Rh	Mo/Mo	Mo/Rh	W/Rh
2 cm	kVp	24.5	25.5	24	26.5	25.5	23	24.5	26	24.5	26	23.5	23.5
	μm	30	25	50	180	115	120	30	25	50	170	120	120
	mAs	8.8	7.1	27.2	138.7	164.9	200.9	9.3	7.0	26.6	137.2	144.1	187.4
3 cm	kVp	25	26.5	26	26.5	28	27.5	25.5	27.5	27	26.5	29.5	31
	μm	30	25	50	135	140	135	30	25	50	130	145	150
	mAs	21.0	13.7	38.8	136.1	133.0	170.9	21.2	12.7	35.7	139.6	126.9	150.2
4 cm	kVp	25.5	27.5	27	26.5	30.5	30	26.5	28.5	28	26	31.5	32
	μm	30	25	50	90	120	115	30	25	50	80	120	120
	mAs	47.5	24.8	65.0	139.0	121.6	152.6	45.2	23.1	60.5	138.0	119.0	146.8
5 cm	kVp	26	28	27.5	26.5	30	30.5	40	30	29	39.5	31	31.5
	μm	30	25	50	45	85	85	30	25	50	20	85	85
	mAs	97.1	46.4	114.5	138.0	123.7	153.7	24.2	38.0	100.0	18.4	120.4	148.9
6 cm	kVp	27	28.5	30.5	30.5	29.5	30.5	41	31	31	40.5	31.5	32.5
	μm	30	25	50	20	50	50	30	25	50	20	55	55
	mAs	98.9	71.4	149.8	46.9	125.9	149.8	25.4	52.9	147.4	19.4	117.6	142.5
7 cm	kVp	35	29	33.5	36	29.5	31.5	41.5	42	33.5	41	31.5	33.5
	μm	30	25	50	20	45	45	30	25	50	20	50	50
	mAs	47.4	75.6	139.6	31.3	127.1	148.7	27.3	23.0	139.6	20.8	116.4	139.6
8 cm	kVp	37.5	29.5	35	37.5	31	31	41	42	42	41	42	42
	μm	30	25	50	20	45	40	30	25	50	20	20	25
	mAs	41.9	79.0	134.3	30.5	119.4	151.6	31.2	25.3	73.8	22.9	21.6	35.7
		Without anitscatter grid											
		Calcification						Tumors					
		fixed filter			variable filter			fixed filter			variable filter		
		Mo/Mo	Mo/Rh	W/Rh	Mo/Mo	Mo/Rh	W/Rh	Mo/Mo	Mo/Rh	W/Rh	Mo/Mo	Mo/Rh	W/Rh
2 cm	kVp	24	24.5	22.5	26	21	21.5	24	24.5	21.5	26	20.5	21
	μm	30	25	50	170	100	105	30	25	50	160	90	95
	mAs	7.5	7.0	32.8	100.9	173.4	209.1	7.9	7.5	47.0	92.9	177.3	216.7
3 cm	kVp	24.5	26	25	26	25	25.5	24.5	27	26	26	27.5	29.5
	μm	30	25	50	140	115	120	30	25	50	135	135	145
	mAs	19.5	13.4	43.0	138.2	139.0	179.8	21.1	12.4	38.9	141.8	133.9	154.9
4 cm	kVp	25	26.5	26.5	25.5	28.5	29	25.5	28	27.5	25.5	30.5	30
	μm	30	25	50	90	110	110	30	25	50	85	115	110
	mAs	47.1	28.1	69.1	142.4	127.5	156.7	48.1	24.3	64.1	146.8	118.8	149.0
5 cm	kVp	25	27.5	27	26	29.5	30	26.5	29.5	28.5	26.5	30.5	29.5
	μm	30	25	50	45	80	80	30	25	50	45	80	75
	mAs	112.3	51.5	128.6	142.4	123.4	154.9	90.8	42.1	111.7	140.8	119.7	159.3
6 cm	kVp	25.5	28	31.5	25.5	30	30	41	30	32	40.5	31.5	32
	μm	30	25	50	35	50	45	30	25	50	20	55	50
	mAs	121.6	76.6	149.2	141.7	122.0	156.2	25.5	59.2	143.6	19.4	117.7	143.6
7 cm	kVp	28.5	28.5	33.5	34.5	29.5	30	41.5	31.5	33.5	40.5	31.5	33.5
	μm	30	25	50	20	45	40	30	25	50	20	50	50
	mAs	93.2	80.8	139.7	35.8	127.1	153.4	27.3	56.6	139.7	21.7	116.5	139.7
8 cm	kVp	37	29	35	37	31	31	14.5	42	42	41	31	42
	μm	30	25	50	20	45	40	30	25	50	20	45	25
	mAs	43.8	84.1	134.3	31.8	119.4	151.6	30.0	25.3	73.9	22.9	119.4	35.8

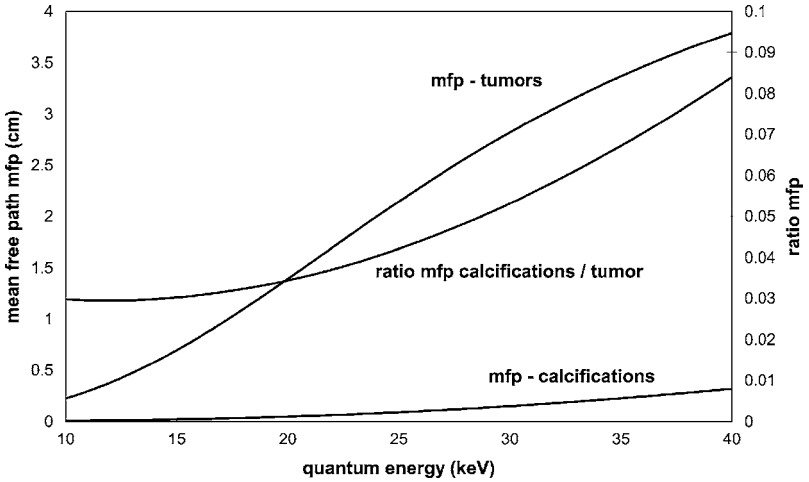

FIG. 18. Mean free path of quanta of different energies for calcifications and tumors as determined by the simulation. Furthermore the ratio between these two functions is given.

The impact of these findings on clinical images still remains to be studied in the future. In addition, new anode/filter combinations for digital mammography may be considered for a further improvement of image quality and a reduction of the patient dose load.

[a]Author to whom correspondence should be addressed. Telephone: +49-09191-18-9746; Fax: +49-09191-18-8951. Electronic mail: philipp.bernhardt@siemens.com

[1]A. C. Thilander-Klang, P. H. R. Ackerholm, I. C. Berlin, N. G. Bjustam, S. L. J. Mattson, L. G. Maanson, C. von Scheele, and S. J. Thunberg, "Influence of anode-filter combinations on image quality and radiation dose in 965 women undergoing mammography," Radiology **203**, 348—354 (1997).

[2]D. R. Dance, A. Thilander-Klang, M. Sandborg, C. L. Skinner, A. Castellano Smith, and G. Alm Carlsson, "Influence of anode/filter material and tube potential on contrast, signal-to-noise ratio and average absorbed dose in mammography: A Monte-Carlo study," Br. J. Radiol. **73**, 1056–1067 (2000).

[3]E. A. Berns, R. E. Hendrick, and G. R. Cutter, "Optimization of technique factors for a silicon diode array full-field digital mammography system and comparison to screen-film mammography with matched average glandular dose," Med. Phys. **30**, 334–340 (2003).

[4]W. Huda, A. M. Sajewicz, K. M. Ogden, and D. R. Dance, "Experimentalinvestigation of the dose and image quality characteristics of a digital mammography imaging system," Med. Phys. **30**, 442–448 (2003).

[5]R. Fahrig and M. J. Yaffe, "Optimization of spectral shape in digital mammography: Dependence on anode material, breast thickness, and lesion type," Med. Phys. **21**, 1473–1481 (1994).

[6]R. Fahrig and M. J. Yaffe, "A model for optimization of spectral shape in digital mammography," Med. Phys. **21**, 1463–1471 (1994).

[7]R. Fahrig, J. A. Rowlands, and M. J. Yaffe, "X-ray imaging with amorphous selenium: Optimal spectra for digital mammography," Med. Phys. **23**, 556–567 (1996).

[8]M. Flynn, C. Dodge, D. Peck, and A. Swinford, "Optimal radiographic techniques for digital mammograms obtained with an amorphous selenium detector," Proc. SPIE **5030**, 147–156 (2003).

[9]J. Y. Lo, E. Samei, J. L. Jesneck, J. T. Dobbins, III, J. A. Baker, S. Singh, R. S. Saunders, and C. E. Floyd, Jr., "Radiographic technique optimization for an amorphous selenium FFDM system: Phantom measurements and initial patient results," in *Proceedings of the 7th International Workshop on Digital Mammography (IWDM 2004)*, edited by E. Pisano (The Biomedical Research Imaging Center, The University of North Carolina at Chapel Hill, Durham, 2005), pp. 31–36.

[10]J. Y. Lo *et al.* (in preparation).

[11]M. J. Yaffe, "Digital Mammography," in *Handbook of Medical Imaging*, edited by J. Beutel, H. L. Kundel, and R. L. Van Metter (SPIE Press, Bellingham, Washington, USA, 2000).

[12]Ph. Bernhardt, L. Baetz, E.-P. Ruehrnschopf, and M. Hoheisel, "Spatial frequency-dependent signal-to-noise ratio as a generalized measure of image quality," Proc. SPIE **5745**, 407–418 (2005).

[13]G. K. Yadava, I. S. Kyprianou, S. Rudin, D. R. Bednarek, and K. R. Hoffmann, "Generalized performance evaluation of x-ray image intensifier compared with a microangiographic system," Proc. SPIE **5745**, 419–429 (2005).

[14]ICRU, "Tissue substitutes in radiation dosimetry and measurement," Report 44 of the International Commission on Radiation Units and Measurements (Bethesda, MD) (1989).

[15]A. D. Maidment, R. Fahrig, and M. J. Yaffe, "Dynamic range requirements in digital mammography," Med. Phys. **20**, 1621–1633 (1993).

[16]P. C. Johns and M. J. Yaffe, "X-ray characterisation of normal and neoplastic breast tissues," Phys. Med. Biol. **32**, 675–695 (1987).

[17]J. M. Boone, T. R. Fewell, and R. J. Jennings, "Molybdenum, rhodium, and tungsten anode spectral models using interpolationg plynomials with application to mammography," Med. Phys. **24**, 1863–1874 (1997).

[18]H. Kharrati and B. Zarrad, "Computation of beam quality parammeters for Mo/Mo, Mo/Rh, Rh/Rh, and W/Al target/filter combinations in mammography," Med. Phys. **30**, 2638–2642 (2003).

[19]T. Mertelmeier, and Ph. Bernhardt, "Scatter in digital mammography: anti-scatter grid versus slot-scanning," Proc. SPIE **5745**, 299–306 (2005).

[20]K. Stierstorfer, T. Flohr, and H. Bruder, "Segmented multiple plane reconstruction: A novel approximate reconstruction scheme for multi-slice spiral CT," Phys. Med. Biol. **7**, 2571–2581 (2002).

[21]A. K. Carton *et al.*, "Contrast visibility of simulated microcalcifications in full field mammography systems," Proc. SPIE **5034**, 412–423 (2003).

[22]D. R. Dance *et al.*, "Monte-Carlo calculation of conversion factors for the estimation of mean glandular breast dose," Phys. Med. Biol. **35**, 1211–1219 (1990).

[23]D. Uhlenbrock, T. Mertelmeier, F. E. Lindhardt, and I. Hilal, "Comparison of x-ray spectra in digital mammography with respect to average glandular dose," abstract submitted to ECR, 2007.

[24]S. Obenauer, K. P. Hermann, and E. Grabbe, "Dose reduction in full-field digital mammography: An anthropomorphic breast phantom study," Br. J. Radiol. **76**, 478–482 (2003).

[25]R. Moeckli, F. R. Verdun, S. Fiedler, M. Pachoud, S. Bulling, P. Schnyder, and J. F. Valley, "Influence of scatter reduction method and monochromatic beams on image quality and dose in mammography," Med. Phys. **30**, 3156–3164 (2003).

[26]D. P. Chakraborty, "The effect of the anti-scatter grid on full-field digital mammography phantom images," J. Digit Imaging **12**, 12–22 (1999).

[27]L. T. Niklason, V. Venkataksishnan, B. H. Opsahl-Ong, and C. E. Landberg, "Anti-scatter grids: Are grids required for digital mammography," abstract #53, presented on RSNA (1998).

[28]W. J. H. Veldkamp, M. A. O. Thijssen, and N. Karssemeijer, "Grid usefulness in direct digital mammography," Abstract #B-0863, presented ECR (2001).

[29]L. Baetz, J. Eser, and T. Mertelmeier, "Detector performance of the new Siemens FFDM system," in *Proceedings of the 7th International Workshop on Digital Mammography (IWDM 2004)*, edited by E. Pisano (The Biomedical Research Imaging Center, The University of North Carolina at Chapel Hill, Durham, 2005), pp. 23–30.